Research article

Feifei Liu*, Meng Wang and Xinping Zhang*

Directional color routing assisted by switchable Fano resonance in bimetallic metagrating

https://doi.org/10.1515/nanoph-2021-0155
Received April 11, 2021; accepted May 31, 2021;
published online June 22, 2021

Abstract: Great progress in nanophotonics has been demonstrated in tailoring the impinging beams. The physics behind those intriguing effects is to a large extent governed by the parameter of the optical phase. While, simple nanostructures usually suffer from fundamental limitations on their efficiency in wave transformation, especially in the transmission system, associated with their inadequate phase accumulation, challenge their implementation in practical application. Here, we describe a transparent nanostructure built from a pair of partially overlapped gold and aluminum semi-nanoshells that show almost π phase accumulation through material-dependent plasmon resonances. Combined with an optical slab waveguide, the bimetallic metagratings exhibit prominent directional color routing properties in transmission light, which result from switchable Fano resonances between plasmon resonances of bimetallic nanostructures and ±1 order waveguide diffraction modes at two opposite oblique incidences due to sufficient phase shift provided by the asymmetric and bimetallic plasmon resonators. Both theoretical and experimental results show that the Fano-resonance-assisted color routing exhibits a relatively broadband tuning range (~150 nm with an efficiency of up to 50%) and a color routing efficiency of up to 70% at the central wavelength of λ = 600 nm.

***Corresponding authors: Feifei Liu**, College Physics & Materials Science, Tianjin Normal University, Tianjin, 300387, China; and Institute of Information Photonics Technology, College of Applied Sciences, Beijng University of Technology, Beijing, 100124, China; and **Xinping Zhang**, Institute of Information Photonics Technology, College of Applied Sciences, Beijng University of Technology, Beijing, 100124, China, E-mail: liufeifei@tjnu.edu.cn (F. Liu); zhangxinping@bjut.edu.cn (X. Zhang). https://orcid.org/0000-0001-5532-2021 (F. Liu). https://orcid.org/0000-0001-6534-0004 (X. Zhang)
Meng Wang, Institute of Information Photonics Technology, College of Applied Sciences, Beijng University of Technology, Beijing, 100124, China; and School of Physical Science and Technology, Inner Mongolia University, Hohhot, Inner Mongolia, 010021, China

Keywords: bimetallic metagrating; directional color routing; optical phase; optical waveguide; plasmon resonance.

1 Introduction

Localized surface plasmon resonances (LSPR) as a result of collective oscillation of free electrons in noble metals has drawn significant interest in the past years, owing to their capability of manipulating light at the nanoscale and owning extremely strong near-field enhancement [1, 2]. Those properties enable the applications of plasmonic nanostructures in improved photovoltaic [3], chemical/biological sensors [4, 5], and surface-enhanced molecular spectroscopies including surface-enhanced Raman scattering [6] and enhanced fluorescence [7]. Meanwhile, plasmonic nanostructures have been also used to control the wavefront [8–10], polarization [11–13] and propagation direction [14–23] of impinging wave to generate strong optical nonlinearities [24], complex vector vortex beam [25], and anomalous refraction and reflection [14, 15]. The latter plasmonic nanostructures including Fano resonance structures typically require coherent oscillations of several plasmonic oscillators with specific phase retardations [17]. For example, the artificial nanoresonators used to produce anomalous refraction or reflection need to support certain phase gradients along the horizontal direction in a super unit cell [14, 15]. Thus, they usually need to be carefully designed and possess relatively complex distributions. Functional nanodevices with ultrathin and simple designs can provide more possibilities for the mass production with simple preparation processes and at a low cost. While, their inadequate phase accumulation by just tuning the size or geometry of the nanodevices [15, 26, 27], makes them usually suffer from fundamental limitations on their efficiency in wave transformation. This challenges their implementation in practical application, especially in the transmission system.

Bimetallic nanoantennas with simple design and large area are proposed in [16], which provide another degree of freedom to manipulate the optical phase in the transparent optical system. In our paper, we investigate such degree of freedom for manipulating the optical phase in metallic

photonic crystal slabs in the transmission direction. As a proof of principle, we experimentally realize the waveguide-bimetallic metagrating, which consists of pairs of partially overlapped gold (Au) and aluminum (Al) semi-nanoshells on a thin optical slab. The calculated and experimental results show that the material-dependent plasmon resonances can produce almost π phase accumulation, which provides conditions for switchable Fano coupling between the plasmon resonances of bimetallic nanostructures and ±1 order waveguide diffraction modes at two opposite oblique incidences. As a result of such an exotic phenomenon, the waveguide-bimetallic metagrating exhibits prominent color routing properties in a direct transmission direction. That is, it is able to directionally sort light of different colors to a direct transmission direction by changing the incident angles from θ to $-\theta$ (see Figure 1). The underlying physics behind this photophysical phenomena is the controllable interference process between direct transmission light (T) and indirect transmission lights corresponding to waveguide diffraction modes modulated by plasmon resonances (W–P) of bimetallic metagrating (see the insets in Figure 1). Moreover, we show that the bimetallic photon-sorting devices can be fabricated over large areas using the low-cost interference lithography and deposition technology. That may facilitate the applications in, for example, tunable passband optical filters, optical sensors, and color holography.

2 Results and discussions

2.1 Realization of the waveguide-bimetallic metagrating

Figure 2(a)–(c) show the fabrication process of the waveguide-bimetallic metagrating. One-dimensional photoresist grating was firstly fabricated as a mask using interference lithography on a glass substrate coated with 200-nm-thick indium-tin-oxide (ITO), as shown in Figure 2(a), where a UV laser at 343 nm and photoresist S1805 (PR) were adopted, the ITO film was acted as an optical waveguide in the investigation of switchable Fano resonances between LSPR of bimetallic metagrating and waveguide modes. The refractive index of the PR film with a thickness of 500 nm and the ITO film was measured by ellipsometry (Horiba UVISEI-2), which was shown as a function of wavelength in Figure S1 in the Supplementary Material. The refractive index of ITO and PR are 1.89 and 1.64, respectively, at the wavelength of 600 nm, which applies well to our simulations. Furthermore, we also measure the transmittance spectrum of the ITO glass as shown in Figure S1. The ITO glass has a very high transmittance in visible light. Then, two metals of Au and Al were deposited sequentially on the surface of the PR mask using two different evaporation angles on opposite sides of

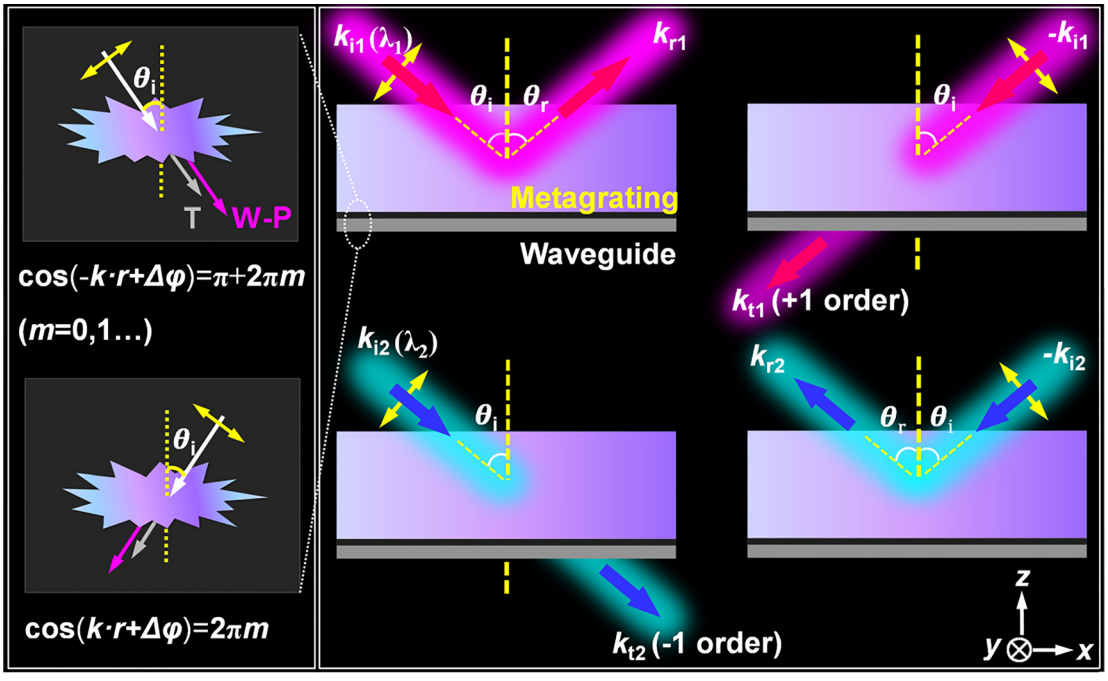

Figure 1: Physical origin and schematic diagrams of the Fano-resonance-assisted directional color routing in waveguide-bimetallic metagrating.

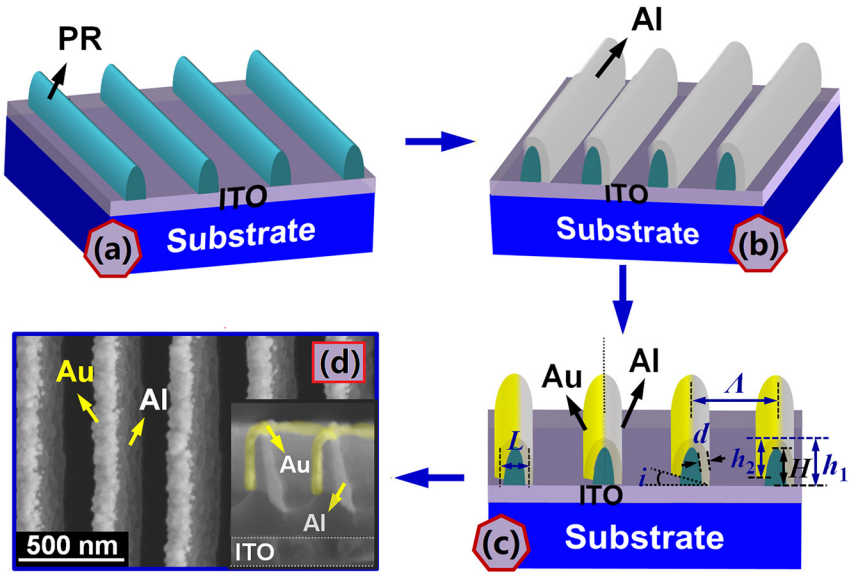

Figure 2: Fabrication procedure of Au–Al bimetallic metagrating.
(a)–(c) Schematic illustration of the fabrication procedure through two-steps oblique thermal evaporation. (d) Scanning electron microscopy images of the Au–Al bimetallic metagrating, inset shows the cross-section profile.

the substrate normal so that the two partially overlapped metallic nanoshells were produced. Refer to the study by F F Liu and X P Zhang [28] for a detailed preparation method of the asymmetric metallic metagrating. In this work, metallic materials of Au and Al are chosen for their different frequency of bulk longitudinal electron excitations and their relatively stable characteristics in the air [29], which enable the bimetallic devices to have a broadband LSPR response with long working life.

The structural parameters of the nanocavities are defined in Figure 2(c): the period of the nanocavity array, Λ; the center-to-center separation between Au and Al semi-nanoshell, L; the modulation depth of the PR grating, H; the height of Al and Au nanoshells, h_1 and h_2, respectively; the thickness of Au and Al nanoshells, d. Asymmetric geometric distribution of Au and Al nanoshells in bimetallic metagrating form an inclined diffraction plane with an angle, i, which provided similar optical properties with that of blazed grating.

Figure 2(d) shows the scanning electron microscopy (SEM) images of the resulting bimetallic metagrating, where the metals of Au and Al can be distinguished by different colors and contrast of the metagrating. The measurement results of the electronic spectrum as shown in Figure S2 confirm further the bimetallic structural design. This method allows for fabrication of metagrating over large areas (centimeter scale) while preserving the structure orientation, size, and composition. The inset in Figure 2(d) shows the cross-section profile of the metagrating, where the period of the metagrating is about $\Lambda = 370$ nm, the modulation depth of the PR grating is about $H = 450$ nm, the height of the Au and Al nanoshells are 335 and 455 nm, respectively, the center-to-center separation between Au and Al nanoshells L is about 155 nm, and the thickness of the Au and Al nanoshells is about 70 nm. Thus, the angle of the inclined diffraction plane formed by asymmetric Au and Al nanoshells i is about 37°.

2.2 Switchable Fano resonances in waveguide-bimetallic metagrating

Figure 3 shows the comparison results of transmission optical extinction spectra of waveguide-bimetallic metagrating in Figure 2(d) between two opposite incidences, where the incident lights are tuned from –10 to 10° with transverse-magnetic (TM) polarization (perpendicular to the extending direction of grating lines). The transmission optical extinction spectrum is the result of the negative logarithm operation of transmittance spectrum (see the equation in *Optical spectroscopy* in Section 4), which enables the comparison spectral results of the switchable Fano resonance at two opposite incidences more clearly. The broadband extinction peaks ranged from 400 to 900 nm correspond to LSPR of bimetallic nanostructures, which can be confirmed by the simulations in below. The angular-tuning extinction features with narrow bandwidth are the Fano resonance between LSPR of bimetallic metagrating and ±1 order waveguide diffraction modes. The central wavelengths of those modes can be roughly estimated by the grating diffraction formulas [30–33]. There are no doubt that two times measurements are the same as the incident angles θ is 0°. Figure 3(a) shows the corresponding spectral responses of the bimetallic metagrating, where the central wavelength of Fano resonances are located at about λ = 600 nm. The little differences in

Figure 3(a) may come from test errors. As increasing the incident angles gradually, we observe pairs of almost complementary extinction features between the spectra at two opposite oblique incident angles of θ_i and $-\theta_i$ both in +1 and −1 order modes, which are highlighted by the pink and blue lines, respectively.

The physics behind such fantastic optical phenomenon is the controllable optical interference processes between direct transmission light and ±1 order waveguide diffraction modes modulated by plasmon resonances of bimetallic metagrating, which allow either constructive interference or destructive interference at two opposite oblique incidences, owing to sufficient phase shift between the asymmetric plasmon resonances of Au and Al nanostructures. Meanwhile, the phase accumulation also provides the conditions for different optical interference processes in +1 and −1 order modes in the waveguide-bimetallic metagrating, which can be distinguished easily from the spectral responses in Figure 3(b)–(f). In a word, we attribute those optical properties above as the switchable Fano resonances in waveguide-bimetallic metagrating. More detailed theoretical analysis of the exotic Fano resonance will be presented in Section 2.3.

2.3 Physical mechanisms for switchable Fano resonances in bimetallic metagrating

2.3.1 Fano resonance in waveguide-monometallic nanostructures

Phase modulation on the initial phase of waveguide diffraction lights by plasmon resonance overturns the interference process between optical waveguide and direct transmission lights to constructive interference in a metallic photonic crystal slab, which is the physical origin of Fano resonance in waveguide-plasmon photonic crystal structures [30, 31, 34]. The Fano resonance in waveguide-plasmon photonic crystal structures opens a narrowband and transmission-enhanced window in direct transmission light [35, 36]. Here, we simplify the waveguide diffraction modes modulated by plasmon resonance to waveguide-plasmon modes. Figure 4 shows the optical diffraction channels of direct transmission or reflective lights, and ±1 order waveguide-plasmon modes in a monometallic photonic crystal slab at an incident angle of θ_i [30, 31], where the high-order diffraction modes are neglected, as they do not

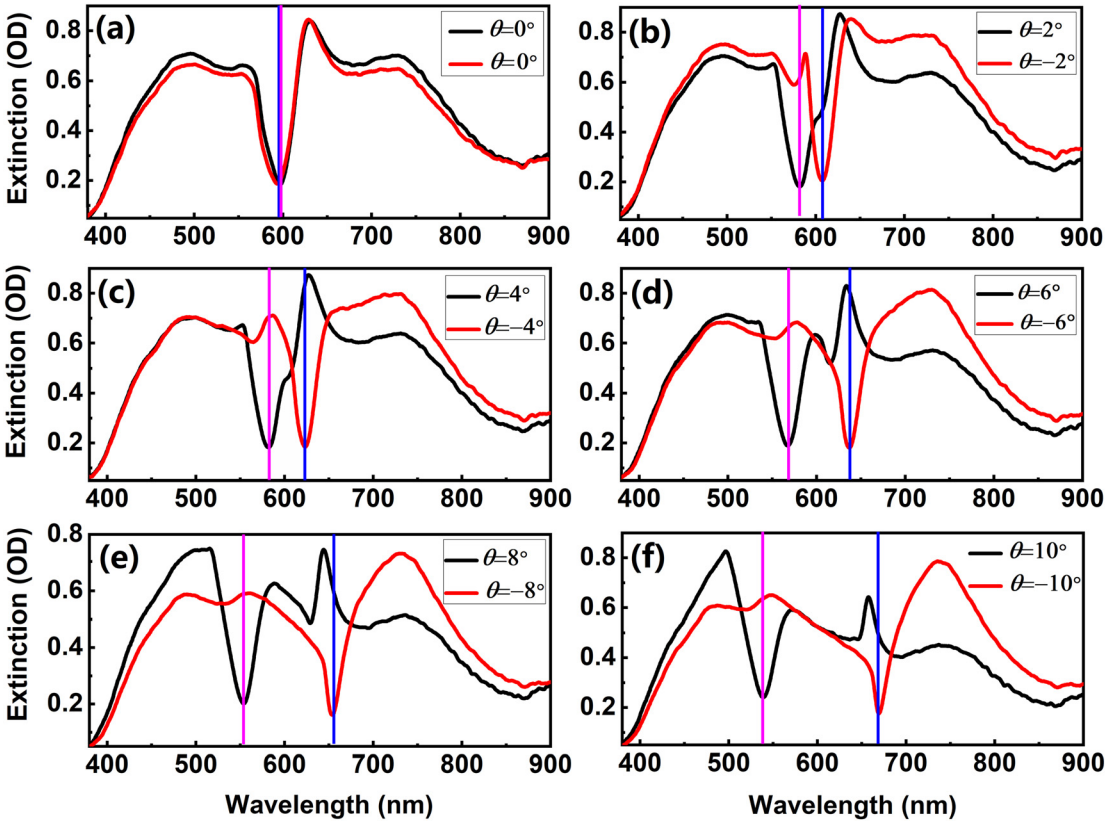

Figure 3: Experimental comparison results of optical extinction spectra of waveguide-bimetallic metagrating between two opposite incidences.

show up in our measurement results in Figure 3. The letters of n_1, n_2, and n_3 in Figure 4 separately denote the refractive index of dielectric layers of air, waveguide slab, and SiO_2 substrate, respectively. The diffraction channels ① and ② colored by black lines with arrows are the direct transmission and reflective lights, respectively, the diffraction channels of ③, ④ and ⑤, ⑥ colored by red and blue lines with arrows denote the +1 and –1 order waveguide-plasmon diffraction modes, respectively, which include the lights in waveguide propagated further and then scattered by Au nanolines. The suspension points denote the lights in waveguide propagated further. The overlap in space between the diffraction beams ①, ③, and ⑤, or the beams of ②, ④, and ⑥ result in optical interference in transmission or reflective directions, respectively. Here, we focus on the optical interference in the transmission direction. The optical intensity of interference terms between direct transmission light and ±1 order waveguide-plasmon diffraction modes in transmission light are proportional to $\cos(k_{+1} n_{12} \Delta L_{+1} + \Delta\varphi_{+1})$ and $\cos(k_{-1} n_{12} \Delta L_{-1} + \Delta\phi_{-1})$, respectively, where k is the free space wave vector, $n_{12}\Delta L$ and $\Delta\varphi$ denote the optical path difference and the initial phase shift between direct transmission light and waveguide-plasmon modes, respectively, n_{12} is the effective refractive index of waveguide and air layers. The ±1 order interference terms mentioned above are usually different for their different resonance wavelengths and the initial phases of waveguide-plasmon modes. While, it is easy to be proved that the total phase shifts between the interference terms at two opposite oblique incidences are the same for both +1 and –1 order diffraction modes ($\cos(-k_{+1} n_{12} \Delta L_{+1} - \Delta\varphi_{+1})$ and $\cos(-k_{-1} n_{12} \Delta L_{-1} - \Delta\phi_{-1})$ for $-\theta_i$). Figure S3 shows the comparison results of optical extinction spectra of Au-coated grating with optical waveguide between two opposite oblique incidences, where the Fano resonances are exactly the same due to almost identical phase shifts at two opposite oblique incidences. Compared with the results as shown in Figure 3, the spectral responses of monometallic grating exhibit relatively low interference efficiency due to the relatively high ohmic loss for the metallic material of gold. Except for that, we also measured the comparison spectral results of monometallic grating with different symmetry, as shown in Figures S4–S7. The asymmetric monometallic gratings in Figures S4 and S6 are decorated with one side of metal like that as shown in Figure 2(b). The asymmetric gratings in Figures S5 and S7 are that similar with bimetallic metagrating. Due to asymmetric diffractions and scattering of the asymmetric metallic grating [37–40], different spectral responses at two opposite incident angles can be distinguished. Such an effect is similar with that in blazed grating. While, the signal contrast for the switchable Fano resonances in such four monometallic structures are relatively weak compared with that in bimetallic metagrating. In the ideal case, we would want the argument of the cosine function to reach to the limit of constructive interference ($kn_{12}\Delta L + \Delta\varphi = 2\pi m, m = 0, \pm1, \pm2\cdots$) for light propagation. Those are the basic characteristics of Fano resonance in waveguide-monometallic photonic crystal systems.

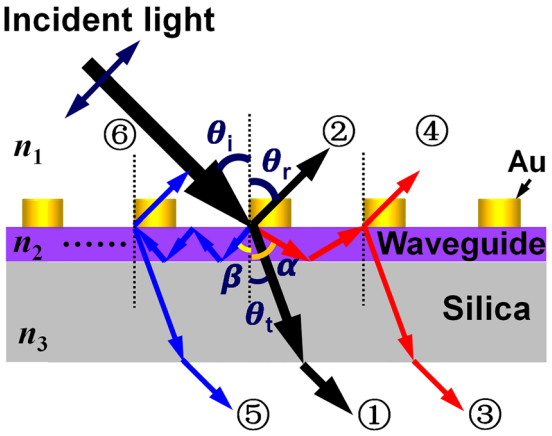

Figure 4: Diffraction process of light in waveguide-monometallic nanograting.

2.3.2 Fano resonance in waveguide-bimetallic metagratings

As to waveguide-bimetallic metagratings, more complicated phase modulations on waveguide modes are involved for increased plasmonic resonators in a structural unit cell [16, 41]. To illuminate the physics behind switchable Fano resonances between waveguide-plasmon diffraction lights and direct transmission light at two opposite oblique incidents, we start from an analytical simulation on two coupled plasmonic resonators of Au and Al semi-nanoshells in bimetallic metagrating without optical waveguide. The design scheme of Au–Al bimetallic nanostructure is exhibited in Figure 5(a), which consists of a pair of partially overlapped Au and Al semi-nanoshells covered on the surface of PR template. Figure 5(b) and (c) show also the sketch maps of Au and Al semi-nanoshell for comparison, where n_4 denotes the refractive index of PR. The location and size of the Au and Al nanoshells can be easily and flexible tuned in experiment.

To evaluate the phase accumulation of Au and Al nanoshells in bimetallic metagrating more accurately, the coupling relationship between such two resonators are

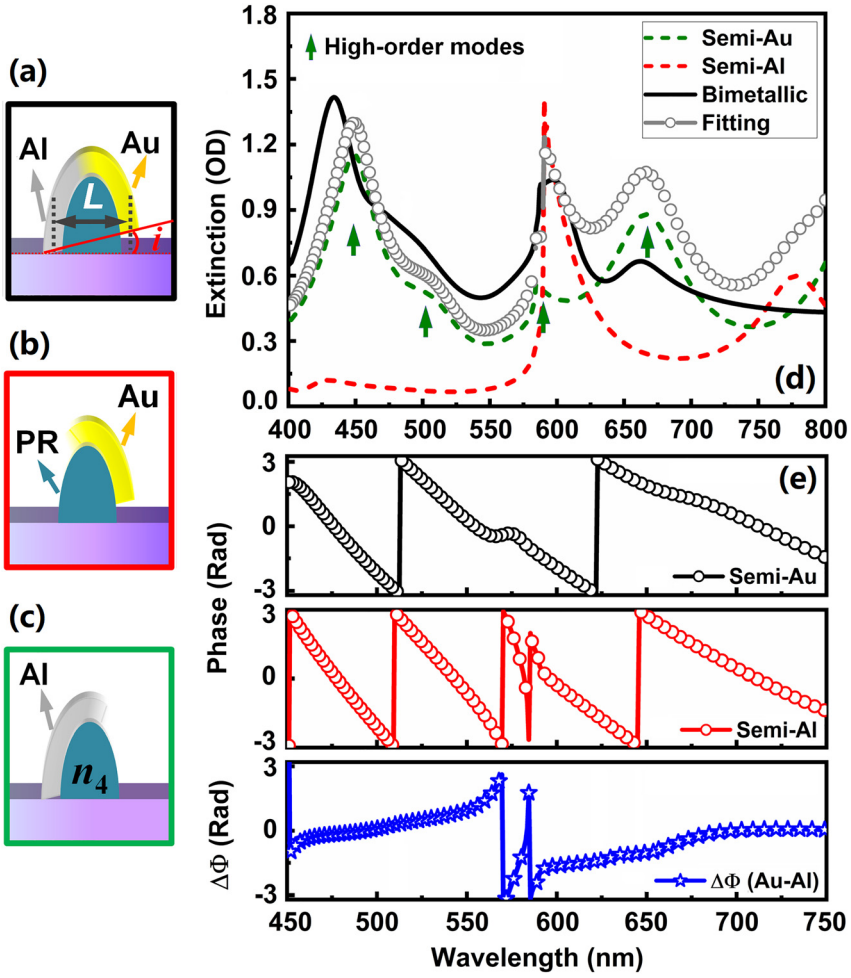

Figure 5: Analytical simulation on Au–Al bimetallic metagrating, semi-Au and semi-Al nanograting, respectively. (a)–(c) Structural designs of Au–Al bimetallic metagrating, semi-Au and semi-Al nanograting, respectively. (d) Transmission optical extinction spectra of different nanogratings in (a)–(c). (e) Phase distributions of semi-Au and semi-Al grating, and the relative phase shift between semi-Au and semi-Al grating.

investigated. Figure 5(d) shows the simulated optical extinction spectra of bimetallic metagrating, Au-semi-nanoshells gratings and Al-semi-nanoshells gratings, as plotted by black solid curve (bimetallic metagrating), green (Au-semi-nanoshells grating, semi-Au grating), and red (Al-semi-nanoshells grating, semi-Al grating) dotted curves, respectively. Some common features as highlighted by green arrows can be observed from the broadband spectral responses of bimetallic and semi-Au grating, which result from multipolar resonances of Au semi-nanoshells (at λ = 445, 500, and 665 nm) and Rayleigh anomalous diffraction of the metallic grating (at λ = 585 nm) (see Figure S8 in Supplementary Material). While, the differences between such two spectra can almost be made up by the resonance mode of Al semi-nanoshells at λ = 600 nm. The little deviations of the resonance wavelengths in bimetallic and semi-Au grating mainly result from different dielectric environments of such two structures. In a word, the simulated spectral results in Figure 5(d) exhibit a relatively weak near-field coupling between Au and Al semi-nanoshells in the bimetallic grating. The fitting curve with a relatively rough method of $E_{\text{fitting}} = W_i E_{\text{Au}} + W_j E_{\text{Al}}$ shows good agreement with the simulated spectrum of bimetallic metagrating, as plotted by grey circles, where E_{fitting} denotes the fitting result of bimetallic metagrating, E_{Au} and E_{Al} denote the extinction spectra of semi-Au and semi-Al grating, respectively, W_i and W_j are the weight to balance the relationship between semi-Au and semi-Al grating. Those to a large extent confirm a fact that the semi-Au and semi-Al nanoshells collectively determine the broadband spectral response of bimetallic nanostructures, while keeping relatively weak coupling. Therefore, the phase accumulation of Au and Al-nanoshells in bimetallic metagrating can be roughly expressed by the phase difference between semi-Au and semi-Al grating.

The reasons for the weak coupling between Au and Al semi-nanoshells in the bimetallic metagrating lie in the following aspects: (1) different wavelengths of the LSPRs of Au and Al semi-nanoshells (Au semi-nanoshells: at λ = 445, 500, and 665 nm, Al semi-nanoshells: at λ = 600 nm); (2) the relatively narrowband properties of the high-order

LSPR of Al semi-nanoshells, which has little overlap in optical spectra with LSPRs of Au semi-nanoshells.

On this basis, we directly simulate the optical phase distributions of semi-Au, semi-Al gratings, and then calculate the phase difference between such two nanostructures. Figure 5(e) shows the corresponding results, which are plotted by black, red, and blue curves with circles, respectively. Multiple phase jumps in different wavelength in the curves plotted by black and red circles are result from phase accumulation of multiple resonances of Au and Al semi-nanoshells, which are wrapped in the range of $[-\pi, \pi]$. Owing mainly to asymmetric material distribution of Au and Al nanoshells, a positive and negative phase shift crossing almost 2π range can be observed at about $\lambda = 570$ nm in the phase-different curve as plotted by blue circles, which provide different initial phase for the waveguide-plasmon modes in different wavelengths, and thus can induce more interesting optical interference processes between waveguide-plasmon modes and direct transmission light.

In waveguide-bimetallic system, the optical interference terms between direct transmission light and ±1 order waveguide-plasmon diffraction lights are determined by both different plasmon resonances of semi-Au and semi-Al nanoshells and their asymmetric geometric distributions. For example, according to the schematic illumination of diffraction channels in Figure 4 and the structural design of bimetallic metagrating in Figure 5(a), the optical intensity of +1 order interference term at incident angles of θ_i can be expressed as:

$$I_{+1}(\theta_i) \propto \cos\left(k_{+1}(n_{12}\Delta L_{+1} + n_{14}L_{+1}) + \Delta\varphi_{\mathrm{Au}+1}\right) + \cos\left(k_{+1}n_{12}\Delta L_{+1} + \Delta\varphi_{\mathrm{Al}+1}\right) \quad (1)$$

Where, $I_{+1}(\theta_i)$ denotes the optical intensity of +1 order interference term, two cosine functions on the right of the formula correspond to the interference terms modulated by Au and Al nanostructures, respectively. $n_{12}\Delta L_{+1}$ and $\Delta\varphi_{\mathrm{Al}+1}$ are the optical path difference and initial phase shift between direct transmission light and waveguide-plasmon modes modulated by Al nanoshells, respectively. $n_{12}\Delta L_{+1} + n_{14}L_{+1}$ and $\Delta\varphi_{\mathrm{Au}+1}$ are that modulated by Au nanoshells, in which the optical path difference of $n_{14}L_{+1}$ is derived from center-to-center separation between Au and Al semi-nanoshells and their asymmetric geometric distribution (see Figure S9(a) in Supplementary Material), n_{14} is effective refractive index of dielectric layers related to the PR and air. In ideal case, the limit of constructive interference for light propagation for +1 order mode happened in the conditions of $k_{+1}(n_{12}\Delta L_{+1} + n_{14}L_{+1}) + \Delta\varphi_{\mathrm{Au}+1} = 2\pi m$ and $k_{+1}n_{12}\Delta L_{+1} + \Delta\varphi_{\mathrm{Al}+1} = 2\pi m$, $m = \pm1, \pm2\cdots$, where $\Delta\varphi = \Delta\varphi_{\mathrm{Au}+1} - \Delta\varphi_{\mathrm{Al}+1}$ is a negative value according to the spectral result in Figure 4(e). Clearly, this requires that the phase shifts of $n_{14}L_{+1}$ is different from zero. Such an ideal case can be satisfied in the bimetallic metagrating through controlling the size, location of the Au and Al nanoshells, and their asymmetric plasmon resonances.

For opposite incident angle of $-\theta_i$, the optical intensity of +1 order interference term can be expressed as:

$$I_{+1}(-\theta_i) \propto \cos\left(k_{+1}n_{12}\Delta L'_{+1} + \Delta\varphi_{\mathrm{Au}+1}\right) + \cos\left(k_{+1}(n_{12}\Delta L'_{+1} + n_{14}L'_{+1}) + \Delta\varphi_{\mathrm{Al}+1}\right) \quad (2)$$

It is different from that in Equation (1), implying different interference characteristics at two opposite oblique incidences. $n_{14}L'_{+1}$ is that derived from center-to-center separation between Au and Al semi-nanoshells and their asymmetric geometric distribution at the incident angle of $-\theta_i$ (see Figure S9(b) in Supplementary Material). Supposing the limit of constructive interferences are reached at the incident angles of θ_i, the ideal destructive interferences can be realized at the angle of $-\theta_i$ in the conditions of $k_{+1}(n_{12}\Delta L'_{+1} + n_{14}L'_{+1}) + \Delta\varphi_{\mathrm{Al}+1} = \pi + 2\pi m$, and $k_{+1}n_{12}\Delta L'_{+1} + \Delta\varphi_{\mathrm{Au}+1} = -\pi + 2\pi m$. Based on those conditions, we can obtain the appropriate values of $n_{14}L'_{+1}$, $n_{14}L_{+1}$ and $\Delta\varphi$ to meet above-mentioned interference processes.

Further calculations show that the ideal phase accumulation between plasmon resonances of semi-Au and semi-Al nanoshells and the optical path difference derived from center-to-center separation between Au and Al semi-nanoshells and their asymmetric geometric distribution for +1 order mode should satisfy $\Delta\varphi = -\pi$ and $k_{+1}n_{14}(L'_{+1} + L_{+1}) = 2\pi$. Those can be realized in the bimetallic metagratings through controlling asymmetric material, geometric distribution of Au and Al nanoshells, and their center-to-center separation. Actually, the interference conditions of the switchable Fano resonance can be relaxed to $3\pi/2 \le \Delta\varphi \le -\pi/2$ and $\pi \le k_{+1}n_{14}(L'_{+1} + L_{+1}) \le 3\pi$. Those are easier to be realized in the bimetallic metagratings. The above analysis process is also suitable for the −1 order interference processes.

In addition, when ±1 order waveguide-plasmon modes are located separately at two sides of the phase jump point between Au and Al nanoshells, different optical interference characteristics can also be found in the ±1 order interference terms in the bimetallic system. According to the schematic diagram of the diffraction channels in Figure 4 and the structural design of bimetallic metagrating in Figure 5(a), the optical intensity of ±1 order interference terms at incident angle of θ_i can be expressed as:

$$\begin{cases} I_{+1} \propto \cos\left(k_{+1}\left(n_{12}\Delta L_{+1} + n_{14}L_{+1}\right) + \Delta\varphi_{\mathrm{Au}+1}\right) + \cos\left(k_{+1}\, n_{12}\Delta L_{+1} + \Delta\varphi_{\mathrm{Al}+1}\right) \\ I_{-1} \propto \cos\left(k_{-1}\, n_{12}\Delta L_{-1} + \Delta\varphi_{\mathrm{Au}-1}\right) + \cos\left(k_{-1}\left(n_{12}\Delta L_{-1} + n_{14}L_{-1}\right) + \Delta\varphi_{\mathrm{Al}-1}\right) \end{cases} \tag{3}$$

It is obvious that the ±1 order interference characteristics are the same with that of +1 order or −1 order interference terms at two opposite oblique incidences. Those are the physics behind the switchable Fano resonances in waveguide-bimetallic metagratings.

The angle-tunable extinction spectra of the waveguide-bimetallic metagrating as shown in Figure 3 exhibit relatively good constructive interference and destructive interference between waveguide-plasmon diffractions and direct transmission light at two opposite oblique incidents. Based on theoretical analysis, such appropriate interference process would be generated at around of $\pi \le k_{+1} n_{14}\left(L'_{+1} + L_{+1}\right) \le 3\pi$ as the ±1 order waveguide-plasmon modes are located in about 600 nm at normal incidence. It has been calculated that the total optical path differences of the bimetallic metagrating in Figure 2(d) at incident angles of $\theta_i \approx 0°$ falls right in that range $\left(k_{+1} n_{14}\left(L'_{+1} + L_{+1}\right) \approx 1.55\pi\right)$. Therefore, the experimental results show good agreement with the theoretical analysis above. Actually, the spectral results of asymmetric monometallic grating in Figures S2–S6 can also verify the theoretical analysis from another point of view.

2.4 Bimetallic metagrating for directional color routing

The switchable Fano resonances in waveguide-bimetallic metagratings can assist such devices in application of directional color routing in the transmission system, which sort only one order of coupled modes into direct transmission direction with a certain incident angle. To characterize the optical performances of the bimetallic color routing, we measure the transmittance spectra of the

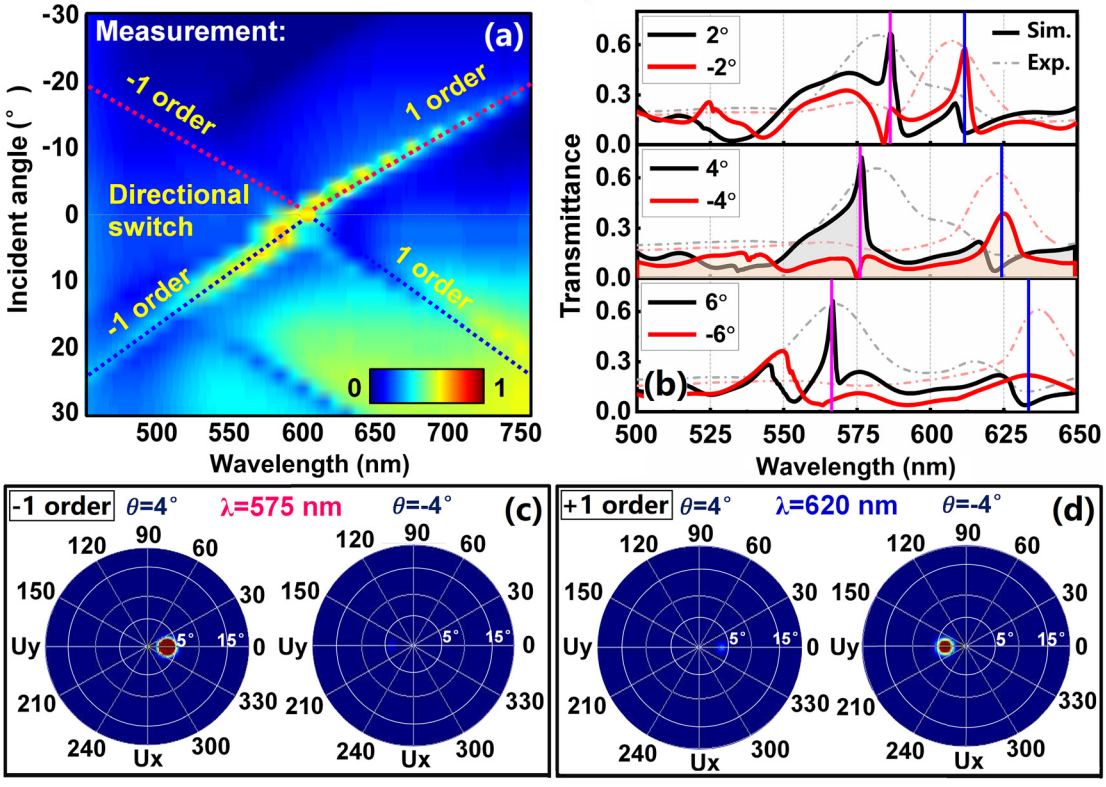

Figure 6: Measurement and calculated optical results of the bimetallic color routing in the transmission direction.
(a) Measurement results of three-dimensional distribution of transmittance optical spectra as a function of wavelength and incident angles. (b) Simulated and experimental transmittance spectra of the bimetallic metagrating tuned from −6 to 6°. (c) Simulated far-field distributions of the bimetallic color routing in transmission direction at incident angles of θ = 4° and −4° and with the wavelengths of λ = 575 and 620 nm.

waveguide-bimetallic metagrating in Figure 2(d) for TM polarization. Figure 6(a) shows the measured three-dimensional distribution of transmittance optical spectra as a function of wavelength and incident angles. As tuning the incident angles from −30 to 30°, we observe a broadband and high-efficiency extinction feature from 450 to 750 nm, corresponding to plasmon resonances of the bimetallic nanostructure, and a series of narrow-band and transmission-enhanced windows in the transmission light, corresponding to the switchable Fano resonances that can sort light of ±1 order coupled modes into different transmission directions. It is worth mentioned that the discrete spectrum spots in Figure 6(a) are resulted from inadequate measurement accuracy of 2° test interval in our optical spectral measurements. For positive incident angles, the transmission-enhanced colored light with wavelengths of λ < 600 nm is sorted into transmission directions, while, the light with wavelengths of λ > 600 nm is assigned to the reflective directions based on the law of conservation of energy. While for negative incident angles, it is precisely opposite. Thus, we name the split line with θ = 0° as the directional switch of the bimetallic color routing. The measurement results show that such a Fano-resonance-assisted color routing exhibits a relatively broadband tuning range from 550 to 700 nm with a color routing efficiency of up to 50% by changing the incident angles. Especially, the color routing efficiency of the bimetallic device can reach up to 70% at the central wavelength of λ = 600 nm.

Simulated transmittance spectra with incident angles tuned from −6 to 6° as shown in Figure 6(b) show good agreement with that in experiment, except for the narrowband resonance properties, where the simulated structural model are designed based on the geometric parameters of SEM image in Figure 5(d), the corresponding experimental results are plotted together with that of simulations with a series of dotted curves. Broadband resonance characteristics in the experiment result from relatively nonuniform structural distribution, which induced lager absorption in practical. It is obvious that such bimetallic color routing exhibits prominent angular-tuning properties. Meanwhile, the almost complementary coupled modes in transmission spectra at two opposite incident angles indicate explicitly the fact that the bimetallic device separately sorts the +1 and −1 order coupling modes into different transmission directions. Figure 6(c) and (d) show the far-field distribution of the bimetallic color routing in transmission direction at incident angles of θ = 4 and −4°, where monochromatic Gaussian beams with the wavelength of λ = 575 and 620 nm are employed as the incident sources. Obviously, the three-dimensional transmission results show more clearly the directionality, efficiency, and wavelength dependence of the bimetallic color routing. Simulated results show good agreement with the experimental results and the theoretical analysis.

3 Conclusions

In summary, we demonstrated a tunable and relatively high-efficiency directional color routing in a material-asymmetric nanostructure in transmission light. The effect originates from the switchable Fano resonances in waveguide-bimetallic metagrating, owing to sufficient phase accumulation through material-dependent plasmon resonances of Au and Al nanoshells. Both experimental and theoretical results verified that the bimetallic color routing exhibits a relatively broadband tuning range from 550 to 700 nm by changing incident angles and a color routing efficiency of up to 70% at the central wavelength of λ = 600 nm. Indeed, such an effect is not limited to the metallic materials of Au and Al, and the nanostructures of one-dimensional nanoshells. Through optimizing the materials or the shape of the resonators, it is likely to observe more broadband and polarization-dependent directional emission. Meanwhile, the material-dependent metagrating as described in this work does not require careful size and geometric design, thus facilitates the fabrication process and the practical application in tunable pass-band optical filters, optical sensors, and color holography.

4 Numerical simulations

The simulations in this work have been performed using finite-difference time-domain (FDTD) solution. For the simulations on transmission optical extinction spectra, electronic-field and charge-density distribution, bloch boundary conditions are applied along the direction perpendicular to the grating lines, perfectly matched layers are assumed along the normal to the grating plane. The incident plane wave is assumed to have a TM polarization. The optical constants for Au and Al are adapted from Johnson and Christy [42]. The whole structures are assumed to be located in a homogeneous medium with a refractive index of n = 1. A mesh size as fine as 2 nm is employed. For the far-field distribution of the bimetallic color routing in the transmission direction, the broadband

plane wave is replaced by a monochromatic Gaussian beam, the periodical structure is set as a quasi-periodic structure with 100 periods.

5 Optical spectroscopy

In the transmission optical spectral measurements, a halogen lamp (HL-2000) is used as the white light source. A USB4000 fiber spectrometer from Ocean Optics is used to measure the transmission spectrum, which has a resolution of 2 nm and an effective spectral band from 340 to 1000 nm. The samples are mounted on a rotation stage with the angular resolution of 1° and a turning range of 360°. The scale of rotation stage is 0° at first as the white light incident normally to the surface of the sample. Then, the rotation stage are tuned to θ and $-\theta$, respectively, with 2° test interval. The optical extinction spectrum is calculated by $-\log_{10}[I(\lambda)/I_0(\lambda)]$, the transmittance spectrum is calculated by $I(\lambda)/I_0(\lambda)$, where $I(\lambda)$ is the transmission spectrum by the sample, $I_0(\lambda)$ is that by a transparent glass with ITO layer arranged in the same geometry. As for high transmittance of ITO glass in visible light, the Fabry-Perot-interference features induced by ITO film are very weak, which can be verified by the transmittance spectrum of the ITO glass in Figure S1. Thus, it is reasonable to use the transmission spectrum of ITO glass as the reference.

Author contributions: All the authors have accepted responsibility for the entire content of this submitted manuscript and approved submission.
Research funding: We acknowledge the National Natural Science Foundation of China (62005197, 61735002, 11274031, 11434016).
Conflict of interest statement: The authors declare no conflicts of interest regarding this article.

References

[1] L. Novotny, *Principles of Nano-Optics*, USA, Cambridge University Press, 2012.
[2] M. C. Daniel and D. Astruc, "Gold nanoparticles: assembly, supramolecular chemistry, quantum-size-related properties, and applications toward biology, catalysis, and nanotechnology," *Chem. Rev.*, vol. 104, pp. 293–346, 2004.
[3] H. A. Atwater and A. Polman, "Plasmonics for improved photovoltaic devices," *Nat. Mater.*, vol. 9, pp. 205–213, 2010.
[4] J. N. Anker, W. P. Hall, O. Lyandres, et al., "Biosensing with plasmonic nanosensors," *Nat. Mater.*, vol. 7, pp. 442–453, 2008.
[5] M. Svedendahl, S. Chen, A. Dmitriev, and M. Käll, "Refractometric sensing using propagating versus localized surface plasmons: A direct comparison," *Nano Lett.*, vol. 9, pp. 4428–4433, 2009.
[6] J. Ye, F. F. Wen, H. Sobhani, et al., "Plasmonic nanoclusters: near field properties of the Fano resonance interrogated with SERS," *Nano Lett.*, vol. 12, pp. 1660–1667, 2012.
[7] P. Anger, P. Bharadwaj, and L. Novotny, "Enhancement and quenching of single molecule fluorescence," *Phys. Rev. Lett.*, vol. 96, p. 113002-1-4, 2006.
[8] A. Pors, M. G. Nielsen, R. L. Eriksen, and S. I. Bozhevolnyi, "Broadband focusing flat mirrors based on plasmonic gradient metasurfaces," *Nano Lett.*, vol. 13, pp. 829–834, 2013.
[9] W. T. Chen, K. Y. Yang, C. M. Wang, et al., "High-efficiency broadband meta-hologram with polarization-controlled dual images," *Nano Lett.*, vol. 14, pp. 225–230, 2014.
[10] S. Y. Yang, Z. Liu, S. Hu, et al., "Spin-selective transmission in chiral folded metasurfaces," *Nano Lett.*, vol. 19, pp. 3432–3439, 2019.
[11] J. M. Hao, Y. Yuan, L. X. Ran, et al., "Manipulating electromagnetic wave polarizations by anisotropic metamaterials," *Phys. Rev. Lett.*, vol. 99, p. 063908-1-4, 2007.
[12] W. J. Sun, Q. He, J. M. Hao, and L. Zhou, "A transparent metamaterial to manipulate electromagnetic wave polarizations," *Opt. Lett.*, vol. 36, pp. 927–929, 2011.
[13] Y. Liang, H. Lin, K. Koshelev, et al., "Full-Stokes polarization perfect absorption with diatomic metasurfaces," *Nano Lett.*, vol. 21, pp. 1090–1095, 2021.
[14] S. L. Sun, K. Y. Yang, C. M. Wang, et al., "High-efficiency broadband anomalous reflection by gradient meta-surfaces," *Nano Lett.*, vol. 12, pp. 6223–6229, 2012.
[15] N. F. Yu, P. Genevet, M. A. Kats, et al., "Light propagation with phase discontinuities: generalized laws of reflection and refraction," *Science*, vol. 334, pp. 333–337, 2011.
[16] T. Shegai, S. Chen, V. D. Miljković, et al., "A bimetallic nanoantenna for directional colour routing," *Nat. Commun.*, vol. 2, p. 481-1-6, 2011.
[17] C. Yan, K. Y. Yang, and O. J. F. Martin, "Fano-resonance-assisted metasurface for color routing," *Light Sci. Appl.*, vol. 6, pp. 1–8, 2017.
[18] W. Liu, A. E. Miroshnichenko, D. N. Neshev, and Y. S. Kivshar, "Broadband unidirectional scattering by magneto-electric core-shell nanoparticles," *ACS Nano*, vol. 6, pp. 5489–5497, 2012.
[19] J. H. Yan, P. Liu, Z. Y. Lin, et al., "Directional Fano resonance in a silicon nanosphere dimer," *ACS Nano*, vol. 9, pp. 2968–2980, 2015.
[20] T. Shibanuma, T. Matsui, T. Roschuk, et al., "Experimental demonstration of tunable directional scattering of visible light from all-dielectric asymmetric dimers," *ACS Photonics*, vol. 4, pp. 489–494, 2017.
[21] T. Coenen, F. B. Arango, A. F. Koenderink, and . Polman, "Directional emission from a single plasmonic scatterer," *Nat. Commun.*, vol. 5, p. 3250-1-8, 2014.
[22] Y. H. Fu, A. I. Kuznetsov, A. E. Miroshnichenko, et al., "Directional visible light scattering by silicon nanoparticles," *Nat. Commun.*, vol. 4, p. 1527-1-6, 2013.
[23] S. P. Gurunarayanan, N. Verellen, V. S. Zharinov, et al., "Electrically driven unidirectional optical nanoantennas," *Nano Lett.*, vol. 17, pp. 7433–7439, 2017.

[24] S. Kim, J. H. Jin, Y. J. Kim, et al., "High-harmonic generation by resonant plasmon field enhancement," *Nature*, vol. 453, pp. 757–760, 2008.
[25] Y. M. Yang, W. Y. Wang, P. Moitra, et al., "Dielectric meta-reflect array for broadband linear polarization conversion and optical vortex generation," *Nano Lett.*, vol. 14, pp. 1394–1399, 2014.
[26] N. F. Yu and F. Capasso, "Flat optics with designer metasurfaces," *Nat. Mater.*, vol. 13, pp. 139–150, 2014.
[27] Z. Y. Zhang, M. Kang, X. Q. Zhang, et al., "Coherent perfect diffraction in metagratings," *Adv. Mater.*, vol. 2002341, pp. 1–6, 2020.
[28] F. F. Liu and X. P. Zhang, "Surface-plasmon-polariton diode by asymmetric plano-concave nanocavities," *Adv. Opt. Mater.*, vol. 6, p. 1701226-1-8, 2018.
[29] F. F. Liu and X. P. Zhang, "Fano coupling between Rayleigh anomaly and localized surface plas- mon resonance for sensor applications," *Biosens. Bioelectron.*, vol. 68, pp. 719–725, 2015.
[30] A. Christ, S. G. Tikhodeev, N. A. Gippius, et al., "Wave-guide-plasmon polaritons: strong coupling of photonic and electronic resonances in a metallic photonic crystal slab," *Phys. Rev. Lett.*, vol. 91, p. 183901-1-4, 2003.
[31] A. Christ, *Optical Properties of Metallic Photonic Crystal Structures*, Marburg, Dissertation an der Philipps-Universität Marburg, 2005.
[32] X. P. Zhang, H. M. Liu, J. R. Tian, et al., "Band-selective optical polarizer based on gold-nanowire plasmonic diffraction gratings," *Nano Lett.*, vol. 8, pp. 2653–2658, 2008.
[33] X. P. Zhang, S. F. Feng, and T. R. Zhai, "Energy transfer channels at the diffraction-anomaly in transparent gratings and applications in sensors," *Photonics Nanostruct.*, vol. 11, pp. 109–114, 2013.
[34] F. F. Liu, X. P. Zhang, X. H. Fang, et al., "Plasmonic microcavity using photo-reduced silver nanoparticles and light-emitting polymer," *Opt. Express*, vol. 24, pp. 1747–1757, 2016.
[35] N. Liu, L. Langguth, T. Weiss, et al., "Plasmonic analogue of electromagnetically induced transparency at the Drude damping limit," *Nat. Mater.*, vol. 8, pp. 758–762, 2009.
[36] N. I. Luk'yanchuk, B. Zheludev, and S. A. Maier, "The Fano resonance in plasmonic nanostructures and metamaterials," *Nat. Mater.*, vol. 9, pp. 707–715, 2010.
[37] X. Y. Wang, C. J. Dai, X. L. Yao, et al., "Asymmetric angular dependence for multicolor display based on plasmonic inclined-nanopillar array," *Nanoscale*, vol. 13, pp. 7273–7278, 2021.
[38] X. C. Wang, A. Diaz-Rubio, V. S. Asadchy, et al., "Extreme asymmetric in metasurfaces via evanescent fields engineering: angular-asymmetric absorption," *Phys. Rev. Lett.*, vol. 121, p. 256802-1-6, 2018.
[39] N. A. Gippius, S. G. Tikhodeev, and T. Ishihara, "Optical properties of photonic crystal slabs with an asymmetrical unit cell," *Phys. Rev. B*, vol. 72, p. 045138-1-7, 2005.
[40] A. Christ, O. J. F. Martin, and Y. Ekinci, "Symmetry breaking in a plasmonic metamaterial at optical wavelength," *Nano Lett.*, vol. 8, pp. 2171–2175, 2008.
[41] J. Zhang and X. P. Zhang, "Bimetallic network with hetero-interfacial plasmons," *Adv. Mater. Interfac.*, vol. 1800580, pp. 1–7, 2018.
[42] P. B. Johnson and R. W. Christy, "Optical constants of the noble metals," *Phys. Rev. B*, vol. 6, pp. 4370–4379, 1972.

Supplementary Material: The online version of this article offers supplementary material (https://doi.org/10.1515/nanoph-2021-0155).